Letter

Imaging Friedel oscillations in rhombohedral trilayer graphene

Long-Jing Yin,[1,3,*] Yue-Ying Zhou,[1,3] Ling-Hui Tong,[1,3] Li-Juan Shi,[1] Zhihui Qin,[1] and Lin He[2]
[1]*School of Physics and Electronics, Hunan University, Changsha 410082, China*
[2]*Center for Advanced Quantum Studies, Department of Physics, Beijing Normal University, Beijing 100875, China*
[3]*Research Institute of Hunan University in Chongqing, Chongqing 401120, China*

(Received 17 August 2022; revised 29 November 2022; accepted 11 January 2023; published 20 January 2023)

Quasiparticle interference-induced spatial standing waves in local density of states, i.e., Friedel oscillations, are first visualized in rhombohedral trilayer graphene (rTG) by using scanning tunneling microscopy and spectroscopy. We show that the long-range standing-wave patterns of rTG can be created not only by the scattering off usual potential barriers including defects and step edges, but also by ABC-ABA stacking domain walls. For step edges as scatterers, both the surface step edge and the underlying step edge can effectively generate quasiparticle standing waves on the surface layer. For all observed types of scatterers in rTG, the Friedel oscillations always exhibit a $1/r$ spatial decay. This decay rate of Friedel oscillations is consistent with that in bilayer graphene, while slower than that in monolayer graphene, directly confirming previous theoretical predictions. Our results provide fundamental knowledge of the nature of scatterers in rTG, which would help us to better understand their microscopic scattering mechanisms.

DOI: 10.1103/PhysRevB.107.L041404

In two-dimensional (2D) electron systems, local potential barriers can be created by localized defects and step edges. The elastic scattering of conduction electrons through these barriers will generate quasiparticle interference, resulting in spatial standing waves in the local density of states (LDOS), also known as Friedel oscillations. Understanding the properties of Friedel oscillations is of primary importance, as it not only can reveal the electronic properties of the material but also access the microscopic scattering mechanisms of its transport devices. Experimentally, quasiparticle Friedel oscillations can be probed by scanning tunneling microscopy and spectroscopy (STM and STS) whose image directly reflects the LDOS on the material surface. The defect and step edge induced spatial LDOS oscillations have both been observed by STM in conventional 2D electron gases such as the noble metal surfaces [1,2]. Friedel oscillations in graphene systems are particularly special. For example, Friedel oscillations in monolayer graphene have a faster decay than that in conventional 2D electron systems, due to the Klein tunneling governed suppression of backscattering [3,4], and bilayer graphene exhibits usual Friedel oscillations with $1/r$ decay [5]. Both of these have been well studied by STM measurements [3,6–8]. Recently, rhombohedral (ABC-stacked) trilayer graphene has been demonstrated to be an interesting system that hosts interesting flat-band-induced correlation phenomena, and thus raises great attention [9–15].

In this Letter, we systematically study the Friedel oscillations of rTG using STM/STS and visualize clear long-range standing waves both near the regular scatterers of defects and step edges and near the unique ABC-ABA stacking domain walls. We demonstrate that both the surface step edge and the underlying step edge can effectively create Friedel oscillations of LDOS on the top layer of rTG. For all types of scatterers observed here, we find that their Friedel oscillations always obey a $1/r$ decay law. This $1/r$ decay is slower than that observed in monolayer graphene, while consistent with that in bilayer graphene. These results directly verify previous theoretical calculations in rhombohedral-stacked graphene [16], offering timely knowledge of the quasiparticle microscopic scattering in rTG.

Our experiments were operated on highly oriented pyrolytic graphite (HOPG, ZYA grade, from SurfaceNet) substrates, which were surface cleaved repeatedly via adhesive tape in air and then delivered immediately into the ultrahigh vacuum STM chamber. The rTG samples are electronically decoupled flakes on top of the HOPG, which can be formed by exfoliation-induced increase of the interlayer spacing or large rotation between them and underlying substrate, as reported in many previous experiments [12,17–20]. The ABC-stacked arrangement of the rTG and its decoupling nature from the substrate were identified by Landau level (LL) spectroscopy [21], as discussed in detail below and in the Supplemental Material [22]. Defects were made by *in situ* sputtering the sample surface with a 500-eV Ar^+-ion beam in an Ar atmosphere of 10^{-9} Torr for 2–3 s. STM/STS measurements were carried out in an ultrahigh vacuum ($\sim 10^{-11}$ Torr), low temperature (~ 4.5 K) UNISOKU STM system under constant-current mode. STM topographic measurements were calibrated against the standard graphene lattice, Si(111) $-$ (7×7) lattice, and Ag(111) surface using Pt/Ir tips. STS spectra were taken by a standard lock-in technique with an ac modulation of 2–10 mV and 793 Hz. STS maps were performed in the constant-height mode.

Figure 1(a) shows a typical STM topographic image of a rTG region on graphite substrate after Ar^+-ion sputtering. The

*Corresponding author: yinlj@hnu.edu.cn

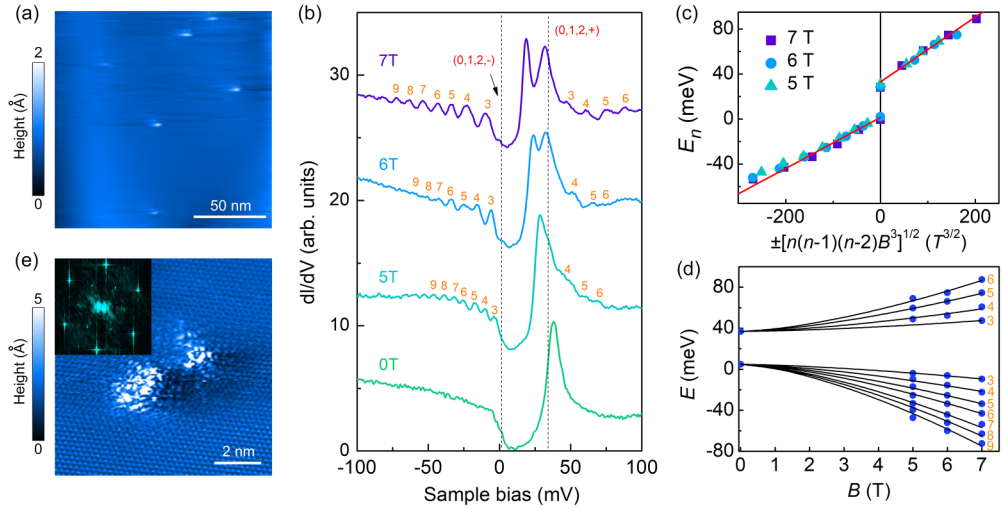

FIG. 1. Identification and characterization of rTG and its defects. (a) STM topographic image ($V_b = 0.4$ V, $I = 0.2$ nA) of a decoupled rTG on graphite surface after Ar^+-ion sputtering. The bright spots correspond to defects. (b) Tunneling spectra ($V_b = 0.3$ V, $I = 0.2$ nA) of the rTG recorded far from the defects under various magnetic fields. LL peak indices are labeled. The curves are offset in y axis for clarity. (c),(d) LL peak energies extracted from (b) plotted versus $\pm[n(n-1)(n-2)B^3]^{1/2}$ (c) and B (d). The solid curves are fits of the data with the theoretical equation. (e) A typical atomic-resolution STM image ($V_b = 0.2$ V, $I = 0.2$ nA) of a defect. Inset: 2D FFT of the STM image.

rTG was identified by STS measurements under various magnetic fields as shown in Figs. 1(b)–1(d). The zero-field dI/dV spectrum of the rTG [Fig. 1(b)] displays an energy gap near the Fermi level, which is generated by inversion symmetry breaking induced by electric field effect from the substrate and tip [17,23,24]. The sharp DOS peak located at the edge of the conduction band originates from the nearly flat band of rTG resided on the top layer, which has been reported previously [12,17,25–27]. The high-magnetic-field STS spectra [Fig. 1(b)] recorded in a defect-free region exhibit high-quality Landau quantization of a gapped rTG. In the simplest tight-binding model considering only nearest intralayer and interlayer coupling, the LL sequences of gapped rTG can be described by $E_n = E_C \pm (2\hbar v_F^2 eB)^{3/2}\sqrt{n(n-1)(n-2)}/\gamma_1^2 \pm E_g/2$, $n = 0, 1, 2\ldots$ (E_C is the energy of the neutrality point, $\pm$ denotes the electron and hole, v_F is the Fermi velocity, e is the electron charge, $\hbar$ is Planck's constant, γ_1 is the nearest-neighbor interlayer hopping strength, and E_g is the energy gap) [28,29]. The extracted energies of the LLs [marked by LL indices in Fig. 1(b)] follow well the above sequences, as shown in Figs. 1(c) and 1(d). From the fit, we obtain $E_g \approx 35$ meV and $\gamma_1 \approx 0.46$ eV, in good agreement with early experiments [12,17,30–32] and theories [33,34]. The well-defined nature of the LLs and their nice fits with theory demonstrate explicitly that the studied sample is a rTG that electronically decoupled from the substrate (see more discussion in [22]).

An important feature visualized in Fig. 1(a) is that pointlike defects can be seen on the rTG surface. These artificially created defects provide a good platform for exploring defect-induced Friedel oscillations in rTG. Figure 1(e) shows a representative atomic-resolution image of a defect in Fig. 1(a) and its corresponding fast Fourier transform (FFT) image. A $(\sqrt{3}\times\sqrt{3})R30^\circ$ pattern (inner six spots) with respect to the graphene reciprocal lattice (outer six spots) is observed in the FFT. This $\sqrt{3}\times\sqrt{3}$ structure arises from the lattice-symmetry-breaking-driven intervalley quasiparticle scattering and is readily observed near graphene defects [3,8,35–37].

We then focus on the intravalley quasiparticle scattering around the defects in rTG. For the intravalley scattering process in graphene, a potential barrier scatters the incident electrons traverse a single constant-energy circle. The incident electrons and the scattered electrons interfere with each other, producing long-range standing waves in the LDOS with a characteristic wavelength given by the scattering wave vector $2k$ (k is the radius of constant-energy circle). This long-range Friedel oscillations can be visualized in the low-bias STM and STS images when the surface is flat enough. Figure 2(a) shows a $-4-$mV STM topographic image measured in the same place as in Fig. 1(a). Long-range spatial oscillations can be seen around the defects even in the topographic image of Fig. 2(a). In order to quantitatively investigate the defect-induced long-range Friedel oscillations in rTG, we performed spatially resolved STS mapping measurements around one single defect under different biases (energies), as shown in Fig. 2(b). The STS maps display obvious long-range standing-wave patterns centered at the defect with an energy-dependent wavelength and a decay away from it. The 2D FFT of these standing-wave images [see the inset of Fig. 2(a) and more data in Fig. S1 [22]] exhibit a clear intravalley scattering ring at the Γ point, indicating an efficient scattering process [3]. Through extracting the scattering wave vector from the FFT, we can deduce the band structure information of rTG. For confirmation of the band structure, we simultaneously plot the band dispersion data extracted from the quasiparticle interference and the LL measurements, as shown in Fig. 2(c). It displays a good consistency between two independent analyses, which together fit well with the tight-binding model of rTG using fitting parameters $\gamma_0 = 3.3$ eV, $\gamma_1 = 0.46$ eV, and $\gamma_4 = -0.099$ eV [22].

We now investigate the spatially extending properties of the defect-induced long-range Friedel oscillations. Figure 2(d)

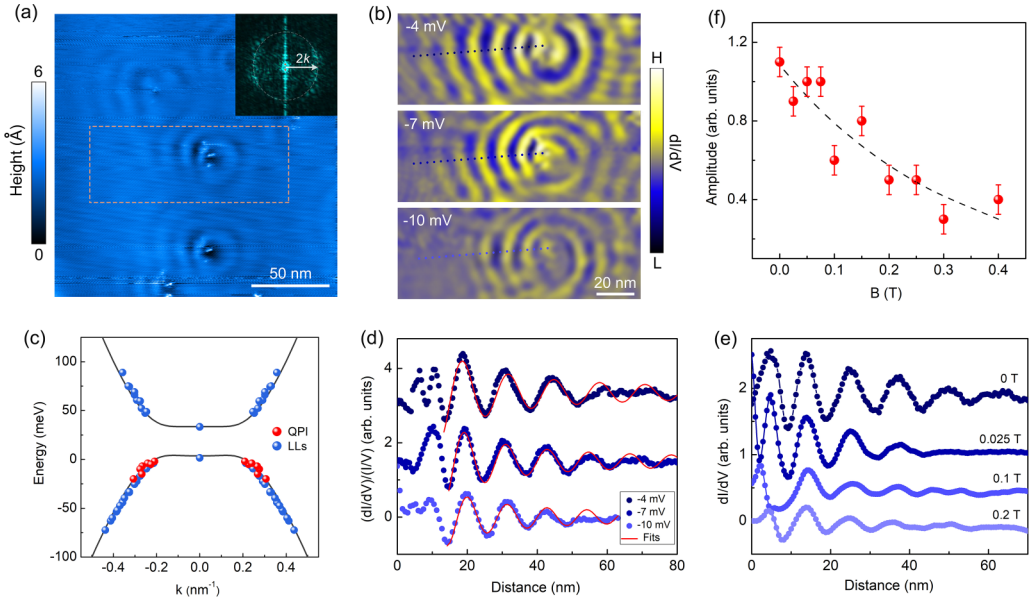

FIG. 2. Defect-induced quasiparticle interference. (a) STM topographic image in the same region of Fig. 1(a) measured under low bias ($V_b = -4$ mV, $I = 50$ pA). Inset shows a typical FFT of the STS map of this region. (b) Energy-dependent STS maps ($I = 50$ pA) of the dashed box area in (a). (c) Effective band dispersion of the rTG. The red dots are momentum vector data obtained from quasiparticle interference (QPI) in (b). The blue dots are obtained from the LL data in Fig. 1 using the semiclassical Onsager quantization condition [12]. The solid curves are tight-binding fits to the data. (d) Normalized dI/dV line cuts starting from the center of the defect obtained from (b). The line cuts are obtained at the positions [dashed lines in (b)] away from other defects to reduce their influence. The red solid lines are fits of the data with $\cos(2kr)/r$. (e) Bias-fixed dI/dV line cuts (-7 mV) around the defect in (b) measured under various magnetic fields. (f) Amplitude of the LDOS oscillations plotted versus magnetic field extracted from (e). The dashed curve is a guide to the eye.

shows dI/dV as a function of the distance from the defect extracted from Fig. 2(b). For all data of different energies, the LDOS oscillations fit well with a function proportional to $\cos(2kr + \delta)/r$ (here r is the distance from the defect center), meaning that the intravalley Friedel oscillations decay as $1/r$ (see Figs. S2 and S3 [22] for more analysis about excluding other possible decay behaviors and avoiding the influence between defects). Similar behavior of the Friedel oscillations is also observed under perpendicular magnetic fields. Figure 2(e) shows spatially dependent dI/dV measured around the same defect in several small magnetic fields. Long-range LDOS oscillations with $1/r$ spatial decay are evident in all magnetic fields, though their amplitude changes. The extracted amplitude of the oscillations decreases with the increase of the magnetic fields, which may originate from the suppression of the Friedel oscillations caused by the electron localization under magnetic fields. Our experiment thus unambiguously demonstrates that the defect-induced long-range Friedel oscillations in rTG exhibit a $1/r$ decay law. This result is quite consistent with the recent theoretical calculations [16].

Next, we explore the behaviors of Friedel oscillations in the scatterer of step edges. Step edge is another usual scatterer in the 2D systems, which can easily generate spatial LDOS oscillations. Figures 3(a) and 3(b) display two types of step edges—the underlying step edge (step edges in the underlying two layers of rTG) and the surface step edge (step edge in the topmost layer)—in rTG. The step type is identified by the atomic image measurements: the graphene lattices of the top layer are continuous across the step edge for the underlying step edge while they are terminated for the surface step edge. The intervalley $(\sqrt{3} \times \sqrt{3})R30^\circ$ scattering is visualized at the surface step edge and is absent at the underlying step edge [lower panels in Figs. 3(a) and 3(b)], corresponding to the nature of the two edges. Interestingly, we observe evident energy- and spatial-dependent long-range LDOS oscillations at both types of step edges, as shown in the STS maps of Figs. 3(c) and 3(d). Such oscillations also can be seen in the bias- and position-evolved dI/dV plot [Fig. 3(e)]. These results indicate that both the surface step edge and the underlying step edge can effectively produce long-range Friedel oscillations on the surface layer of rTG, verifying previous prediction [16]. By fitting the dI/dV line cuts of the standing waves, we obtain the $1/r$-decaying Friedel oscillations for the scatterers of both step edges [Figs. 3(d) and 3(f), and see more analysis in Figs. S4–S6 [22]], which is in line with the situation of the defect scatterer.

Besides the regular local defects and step edges, the stacking domain-wall soliton—an interlayer stacking dislocation—also easily exists in multilayer graphene [19,24,30,38,39]. For trilayer graphene, the most common stacking soliton is ABC-ABA stacking domain wall—the boundary separates rhombohedral and Bernal stacking configurations without lattice breaking. Such ABC-ABA domain walls have been recently demonstrated to exhibit interesting electronic and optical properties [24,30,40]. In the following, we study whether the ABC-ABA domain walls can generate Friedel oscillations. Figure 4(a) shows an observed ABC-ABA domain wall (marked by the dashed line) in a trilayer graphene. The ABC-ABA domain wall is identified by the STS according to the distinct band structures of ABC- and ABA-stacked graphene. For ABC-stacked trilayer graphene, it features a sharp flat-band peak near the Fermi energy in the dI/dV

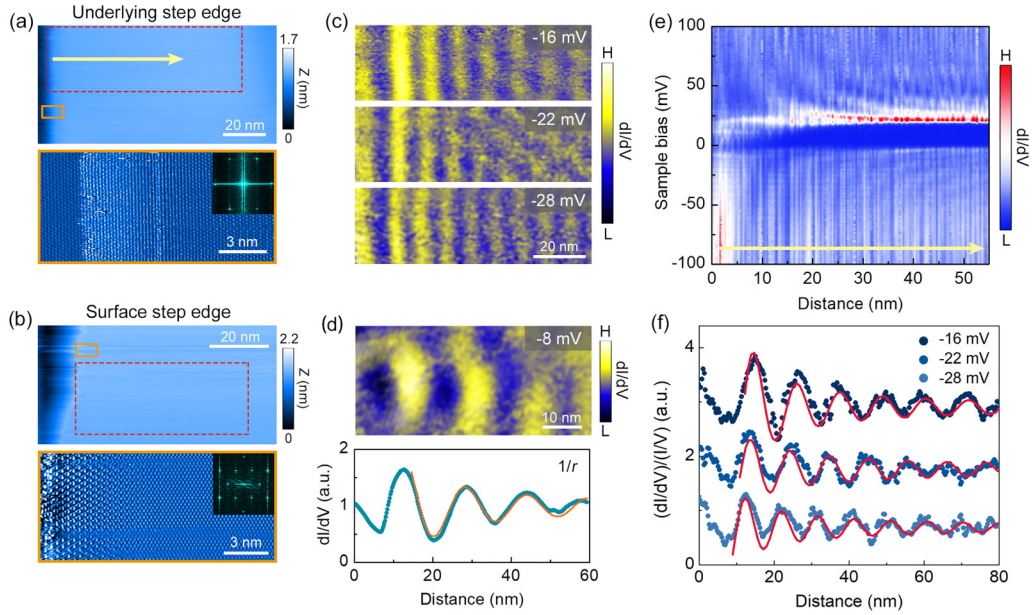

FIG. 3. Quasiparticle interference near step edges. (a),(b) Upper panels: STM topographic images around an underlying step edge (a) and a surface step edge (b) in two different rTG samples. Lower panels: atomic-resolution STM images of the step edges at the positions marked by the frames in corresponding upper panels. Insets are the FFT of the images. The top graphene lattices are continuous across the step edge in (a), indicating that the step edge is in the underlying layers. (a) $V_b = 0.15$ V, $I = 0.2$ nA; (b) $V_b = 0.2$ V, $I = 0.3$ nA. (c) Spectroscopic maps of the dashed square area in (a) at -16 meV, -22 meV, and -28 meV ($I = 0.1$ nA). (d) STS map of the dashed square area in (b) at -8 meV ($I = 0.1$ nA) and its averaged line profile. (e) Contour plot of spatially resolved dI/dV spectra ($V_b = 0.15$ V, $I = 0.2$ nA) recorded along the arrow in (a). (f) LDOS oscillation line cuts from (c). The solid lines in (d) and (f) are fits of the data with $\cos(2kr)/r$.

curve, as discussed in Fig. 1. For ABA-stacked trilayer, it has a V-shaped STS spectrum [18,30,41]. Figure 4(b) presents the position-evolved dI/dV spectra across the ABC-ABA domain wall. It displays a smooth transition from the flat-band spectrum (ABC) to the V-shaped spectrum (ABA), confirming the existence of an ABC-ABA domain wall [24,30]. The obtained

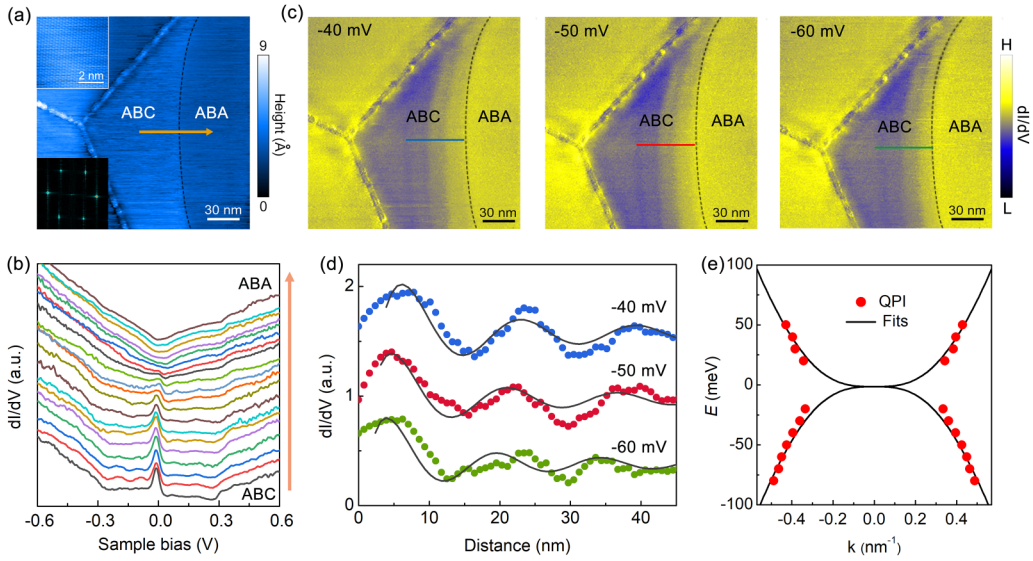

FIG. 4. Quasiparticle interference near an ABC-ABA domain wall. (a) STM topographic image ($V_b = 30$ mV, $I = 0.2$ nA) of an ABC-ABA domain-wall region on graphite. The dashed curve indicates the domain wall. The Y-shaped 1D structures in the left side of ABC region are grain boundaries. These grain boundaries could also induce Friedel oscillations (see Fig. S8 [22]). Insets show the atomic-resolution image of the domain wall and its FFT. (b) dI/dV spectra ($V_b = 0.3$ V, $I = 0.2$ nA) across the domain wall along the blue arrow in (a). (c) dI/dV spatial maps at different energies -40, -50, and -60 meV ($I = 0.2$ nA) over the region in (a). (d) dI/dV line cuts along the colored lines in (c) showing LDOS oscillations in the ABC side. The solid lines are curve fits of the data with $\cos(2kr)/r$. (e) Effective band structure of the ABC-stacked trilayer graphene. The solid curves are tight-binding fits to the data, which yield $\gamma_0 = 2.9$ eV, $\gamma_1 = 0.53$ eV, and $\gamma_4 = 0.03$ eV.

FFT of the atomic resolution image at the ABC-ABA domain wall only exhibits a 1×1 graphene lattice [insets in Fig. 4(a)], indicating the absence of the intervalley scattering at the domain wall. This result is consistent with that observed in bilayer graphene stacking domain walls [42]. We then investigate the intravalley scattering by performing large area energy-fixed STS mapping measurement in this ABC-ABA domain-wall region. Figure 4(c) shows three representative STS maps at negative energies for the same region as in Fig. 4(a). Remarkably, long-wavelength LDOS oscillations are observed in the ABC side with the standing waves parallel to the domain wall and decay moving away from it. To examine the nature of the oscillations, we plot the dI/dV as a function of distance from the domain wall for the energies of Fig. 4(c), as shown in Fig. 4(d). The curves also display good fits of $\cos(2kr + \delta)/r$ (see Figs. S7–S10 [22] for more data and similar results in another sample). From the fits, we extract the wave vector of the oscillations and nicely reproduce the effective band dispersion of the rTG [Fig. 4(e)], affirming the intravalley scattering origin of the oscillations. The above results thus demonstrate that although the ABC-ABA stacking domain wall does not introduce intervalley scattering, it could generate intravalley-scattering-induced long-range Friedel oscillations in rTG which also obey a $1/r$ decay law. It is worth noting that we did not observe clear oscillations in the ABA side of the ABC-ABA domain wall [see Fig. 4(c) and Figs. S8 and S9 [22]]. This phenomenon may be related to the multicomponent low-energy band structures of ABA trilayer graphene [18,30,41] which could introduce the mixing of different types of Friedel oscillations and thus weaken the total oscillations.

It has been demonstrated that monolayer graphene has a faster decay of the Friedel oscillations than in conventional 2D electron systems, due to the Klein tunneling induced suppression of backscattering [3]. For example, theoretical calculations obtained $1/r^2$-decaying Friedel oscillations around impurity defects [4,5] and STM experiment observed a $1/r^{3/2}$ decay of LDOS oscillations near step edges [6] in monolayer graphene. For bilayer graphene, however, theory and experiment both demonstrated the normal Friedel oscillations with a $1/r$ decay [5,7]. Our experiment indicates that both the regular scatterers—defects and step edges—and the unique ABC-ABA stacking domain walls can create remarkable long-range Friedel oscillations in rTG which aways show a $1/r$ spatial decay similar to the bilayer case.

In conclusion, by using STM and STS measurements, we have imaged clear long-range Friedel oscillations in ABC-stacked trilayer graphene near the regular scatterers of defects and step edges, as well as near the unique ABC-ABA stacking domain walls. We found that for all types of scatterers observed here, the Friedel oscillations of rTG always exhibit a $1/r$ spatial decay. Our work gives insight into the nature of scatterers in rTG and provides fundamental understanding of their microscopic scattering behaviors.

This work was supported by the National Natural Science Foundation of China (Grants No. 12174095, No. 12141401, No. 11974050, and No. 12174096), the Natural Science Foundation of Hunan Province, China (Grant No. 2021JJ20026), and the Strategic Priority Research Program of Chinese Academy of Sciences (Grant No. XDB30000000). L.J.Y. also acknowledges support from the Science and Technology Innovation Program of Hunan Province, China (Grant No. 2021RC3037) and the Natural Science Foundation of Chongqing, China (Grant No. cstc2021jcyj-msxmX0381). The authors acknowledge the financial support from the Fundamental Research Funds for the Central Universities of China.

[1] M. F. Crommie, C. P. Lutz, and D. M. Eigler, Imaging standing waves in a two-dimensional electron gas, Nature (London) **363**, 524 (1993).

[2] Y. Hasegawa and P. Avouris, Direct Observation of Standing Wave Formation at Surface Steps Using Scanning Tunneling Spectroscopy, Phys. Rev. Lett. **71**, 1071 (1993).

[3] I. Brihuega, P. Mallet, C. Bena, S. Bose, C. Michaelis, L. Vitali, F. Varchon, L. Magaud, K. Kern, and J. Y. Veuillen, Quasiparticle Chirality in Epitaxial Graphene Probed at the Nanometer Scale, Phys. Rev. Lett. **101**, 206802 (2008).

[4] V. V. Cheianov and V. I. Fal'ko, Friedel Oscillations, Impurity Scattering, and Temperature Dependence of Resistivity in Graphene, Phys. Rev. Lett. **97**, 226801 (2006).

[5] C. Bena, Effect of a Single Localized Impurity on the Local Density of States in Monolayer and Bilayer Graphene, Phys. Rev. Lett. **100**, 076601 (2008).

[6] J. Xue, J. Sanchez-Yamagishi, K. Watanabe, T. Taniguchi, P. Jarillo-Herrero, and B. J. LeRoy, Long-Wavelength Local Density of States Oscillations Near Graphene Step Edges, Phys. Rev. Lett. **108**, 016801 (2012).

[7] M. Yankowitz, J. I. J. Wang, S. Li, A. G. Birdwell, Y.-A. Chen, K. Watanabe, T. Taniguchi, S. Y. Quek, P. Jarillo-Herrero, and B. J. LeRoy, Band structure mapping of bilayer graphene via quasiparticle scattering, APL Mater. **2**, 092503 (2014).

[8] G. M. Rutter, J. N. Crain, N. P. Guisinger, T. Li, P. N. First, and J. A. Stroscio, Scattering and interference in epitaxial graphene, Science **317**, 219 (2007).

[9] G. Chen, A. L. Sharpe, P. Gallagher, I. T. Rosen, E. J. Fox, L. Jiang, B. Lyu, H. Li, K. Watanabe, T. Taniguchi, J. Jung, Z. Shi, D. Goldhaber-Gordon, Y. Zhang, and F. Wang, Signatures of tunable superconductivity in a trilayer graphene moire superlattice, Nature (London) **572**, 215 (2019).

[10] G. Chen, L. Jiang, S. Wu, B. Lyu, H. Li, B. L. Chittari, K. Watanabe, T. Taniguchi, Z. Shi, J. Jung, Y. Zhang, and F. Wang, Evidence of a gate-tunable Mott insulator in a trilayer graphene moiré superlattice, Nat. Phys. **15**, 237 (2019).

[11] B. L. Chittari, G. Chen, Y. Zhang, F. Wang, and J. Jung, Gate-Tunable Topological Flat Bands in Trilayer Graphene Boron-Nitride Moiré Superlattices, Phys. Rev. Lett. **122**, 016401 (2019).

[12] L.-J. Yin, L.-J. Shi, S.-Y. Li, Y. Zhang, Z.-H. Guo, and L. He, High-Magnetic-Field Tunneling Spectra of ABC-Stacked Trilayer Graphene on Graphite, Phys. Rev. Lett. **122**, 146802 (2019).

[13] H. Zhou, T. Xie, T. Taniguchi, K. Watanabe, and A. F. Young, Superconductivity in rhombohedral trilayer graphene, Nature (London) **598**, 434 (2021).

[14] H. Zhou, T. Xie, A. Ghazaryan, T. Holder, J. R. Ehrets, E. M. Spanton, T. Taniguchi, K. Watanabe, E. Berg, M. Serbyn, and A. F. Young, Half- and quarter-metals in rhombohedral trilayer graphene, Nature (London) **598**, 429 (2021).

[15] J. Yang, G. Chen, T. Han, Q. Zhang, Y.-H. Zhang, L. Jiang, B. Lyu, H. Li, K. Watanabe, T. Taniguchi, Z. Shi, T. Senthil, Y. Zhang, F. Wang, and L. Ju, Spectroscopy signatures of electron correlations in a trilayer graphene/hBN moiré superlattice, Science **375**, 6586 (2022).

[16] C. Dutreix and M. I. Katsnelson, Friedel oscillations at the surfaces of rhombohedral N-layer graphene, Phys. Rev. B **93**, 035413 (2016).

[17] L.-J. Yin, L.-Z. Yang, L. Zhang, Q. Wu, X. Fu, L.-H. Tong, G. Yang, Y. Tian, L. Zhang, and Z. Qin, Imaging of nearly flat band induced atomic-scale negative differential conductivity in ABC-stacked trilayer graphene, Phys. Rev. B **102**, 241403(R) (2020).

[18] L.-J. Yin, S.-Y. Li, J.-B. Qiao, J.-C. Nie, and L. He, Landau quantization in graphene monolayer, Bernal bilayer, and Bernal trilayer on graphite surface, Phys. Rev. B **91**, 115405 (2015).

[19] L.-J. Yin, H. Jiang, J.-B. Qiao, and L. He, Direct imaging of topological edge states at a bilayer graphene domain wall, Nat. Commun. **7**, 11760 (2016).

[20] G. Li, A. Luican, and E. Y. Andrei, Scanning Tunneling Spectroscopy of Graphene on Graphite, Phys. Rev. Lett. **102**, 176804 (2009).

[21] L.-J. Yin, K.-K. Bai, W.-X. Wang, S.-Y. Li, Y. Zhang, and L. He, Landau quantization of Dirac fermions in graphene and its multilayers, Front. Phys. **12**, 127208 (2017).

[22] See Supplemental Material at http://link.aps.org/supplemental/10.1103/PhysRevB.107.L041404 for more experimental data and analysis.

[23] Y.-P. Wang, X.-G. Li, J. N. Fry, and H.-P. Cheng, First-principles studies of electric field effects on the electronic structure of trilayer graphene, Phys. Rev. B **94**, 165428 (2016).

[24] M. Yankowitz, J. I. Wang, A. G. Birdwell, Y. A. Chen, K. Watanabe, T. Taniguchi, P. Jacquod, P. San-Jose, P. Jarillo-Herrero, and B. J. LeRoy, Electric field control of soliton motion and stacking in trilayer graphene, Nat. Mater. **13**, 786 (2014).

[25] A. Kerelsky, C. Rubio-Verdú, L. Xian, D. M. Kennes, D. Halbertal, N. Finney, L. Song, S. Turkel, L. Wang, K. Watanabe, T. Taniguchi, J. Hone, C. R. Dean, D. N. Basov, A. Rubio, and A. N. Pasupathy, Moiréless correlations in ABCA graphene, Proc. Natl. Acad. Sci. USA **118**, e2017366118 (2021).

[26] R. Xu, L.-J. Yin, J.-B. Qiao, K.-K. Bai, J.-C. Nie, and L. He, Direct probing of the stacking order and electronic spectrum of rhombohedral trilayer graphene with scanning tunneling microscopy, Phys. Rev. B **91**, 035410 (2015).

[27] D. Pierucci, H. Sediri, M. Hajlaoui, J.-C. Girard, T. Brumme, M. Calandra, E. Velez-Fort, G. Patriarche, M. G. Sill, G. Ferro, V. Soulière, M. Marangolo, F. Sirotti, F. Mauri, and A. Ouerghi, Evidence for flat bands near the fermi level in epitaxial rhombohedral multilayer graphene, ACS Nano **9**, 5432 (2015).

[28] M. Koshino and E. McCann, Trigonal warping and Berry's phase Nπ in ABC-stacked multilayer graphene, Phys. Rev. B **80**, 165409 (2009).

[29] S. Yuan, R. Roldán, and M. I. Katsnelson, Landau level spectrum of ABA- and ABC-stacked trilayer graphene, Phys. Rev. B **84**, 125455 (2011).

[30] L.-J. Yin, W.-X. Wang, Y. Zhang, Y.-Y. Ou, H.-T. Zhang, C.-Y. Shen, and L. He, Observation of chirality transition of quasiparticles at stacking solitons in trilayer graphene, Phys. Rev. B **95**, 081402(R) (2017).

[31] M. Yankowitz, F. Wang, C. N. Lau, and B. J. LeRoy, Local spectroscopy of the electrically tunable band gap in trilayer graphene, Phys. Rev. B **87**, 165102 (2013).

[32] L. Zhang, Y. Zhang, J. Camacho, M. Khodas, and I. Zaliznyak, The experimental observation of quantum Hall effect of $l = 3$ chiral quasiparticles in trilayer graphene, Nat. Phys. **7**, 953 (2011).

[33] F. Zhang, B. Sahu, H. Min, and A. H. MacDonald, Band structure of ABC-stacked graphene trilayers, Phys. Rev. B **82**, 035409 (2010).

[34] N. B. Kopnin, M. Ijäs, A. Harju, and T. T. Heikkilä, High-temperature surface superconductivity in rhombohedral graphite, Phys. Rev. B **87**, 140503(R) (2013).

[35] C. Dutreix, H. Gonzalez-Herrero, I. Brihuega, M. I. Katsnelson, C. Chapelier, and V. T. Renard, Measuring the Berry phase of graphene from wavefront dislocations in Friedel oscillations, Nature (London) **574**, 219 (2019).

[36] Y. Zhang, Y. Su, and L. He, Local Berry Phase Signatures of Bilayer Graphene in Intervalley Quantum Interference, Phys. Rev. Lett. **125**, 116804 (2020).

[37] Y. Niimi, H. Kambara, and H. Fukuyama, Localized Distributions of Quasi-Two-Dimensional Electronic States Near Defects Artificially Created at Graphite Surfaces in Magnetic Fields, Phys. Rev. Lett. **102**, 026803 (2009).

[38] J. S. Alden, A. W. Tsen, P. Y. Huang, R. Hovden, L. Brown, J. Park, D. A. Muller, and P. L. McEuen, Strain solitons and topological defects in bilayer graphene, Proc. Natl. Acad. Sci. USA **110**, 11256 (2013).

[39] L. Jiang, S. Wang, Z. Shi, C. Jin, M. I. B. Utama, S. Zhao, Y. R. Shen, H. J. Gao, G. Zhang, and F. Wang, Manipulation of domain-wall solitons in bi- and trilayer graphene, Nat. Nanotechnol. **13**, 204 (2018).

[40] J. Zhang, J. Han, G. Peng, X. Yang, X. Yuan, Y. Li, J. Chen, W. Xu, K. Liu, Z. Zhu, W. Cao, Z. Han, J. Dai, M. Zhu, S. Qin, and K. S. Novoselov, Light-induced irreversible structural phase transition in trilayer graphene, Light Sci. Appl. **9**, 174 (2020).

[41] Y. Zhang, J.-B. Qiao, L.-J. Yin, and L. He, High-resolution tunneling spectroscopy of ABA-stacked trilayer graphene, Phys. Rev. B **98**, 045413 (2018).

[42] J. D. Verbakel, Q. Yao, K. Sotthewes, and H. J. W. Zandvliet, Valley-protected one-dimensional states in small-angle twisted bilayer graphene, Phys. Rev. B **103**, 165134 (2021).